Ab Initio Density Functional Computations of Conformations and Bond Dissociation Energies for Hexahydro-1,3,5-trinitro-1,3,5-triazine

Nathan J. Harris* and Koop Lammertsma*

Contribution from the Departments of Chemistry, University of Alabama at Birmingham, Birmingham, Alabama 35294, and Vrije Universiteit, 1081 HV Amsterdam, The Netherlands

Received February 9, 1997[⊗]

Abstract: Ab initio computations are described of the conformers and bond dissociation energies of hexahydro-1,3,5-trinitro-1,3,5-triazine (RDX) with the Becke3-Lee-Yang-Parr (B3LYP) nonlocal density functional and the standard 6-31G* and 6-311G** Gaussian basis sets. Five conformational minima, closely spaced in energy, were located at the B3LYP/6-31G* level of theory. The experimental gas-phase and solid-phase geometries for RDX are compared with the B3LYP/6-31G* geometries. The rather short N−N bonds in the experimental crystal structure suggest that intermolecular interactions lead to enhanced donation of the amine lone pair into the nitro group in the solid state. The RDX nitrogen and carbon radicals have key roles in thermal decomposition of RDX. The B3LYP/6-311G** computed estimates for the N−NO$_2$ and the C−H dissociation energies (D_o) in RDX are respectively 42 and 85 kcal/mol. Compared with computed N−NO$_2$ and C−H bond strengths in related molecules, the bonds in RDX are rather weak. This suggests that initiation of decomposition by N−N cleavage and propagation of the decomposition by hydrogen atom transfers should be facile.

Introduction

Numerous experimental studies show that N−NO$_2$ bond homolysis is the initial step in the thermal decomposition of hexahydro-1,3,5-trinitro-1,3,5-triazine (RDX) and other nitramines.[1] The N−NO$_2$ homolysis was found to compete with ring fission in the infrared multiphoton dissociation (IRMPD) of RDX in a molecular beam.[2] In fact, the concerted fission to CH$_2$NNO$_2$ was found to be the primary channel for the unimolecular decomposition, but this seems to be the only instance in which the concerted fission has been observed. The N−NO$_2$ fission was the exclusive initial step in the RDX decomposition induced by pulsed CO$_2$ laser pyrolysis.[3] Decomposition of RDX in dilute acetone solution (240 °C, 40 s) gave predominantly the mononitroso product, resulting from substitution of NO for NO$_2$.[4] This result was interpreted mechanistically as N−NO$_2$ cleavage followed by combination of the RDX and NO radicals. The mononitroso product was also formed in low yield from slow pyrolysis of neat RDX.

The N−NO$_2$ homolysis also takes place in the UV photolysis of RDX. The NO$_2$ radicals from photolysis of crystalline RDX have been observed by electron paramagnetic resonance (EPR) spectroscopy.[5] In addition, the dimerization product (N$_2$O$_4$) has been observed from FTIR spectroscopic study of UV photolyzed RDX.[6] The NO$_2$ and amine radicals generated by N−NO$_2$ cleavage can recombine to give an isomerized *N*-nitrite.[7] This

pathway has been observed by EPR spectroscopy for low-temperature photolysis of crystalline RDX and hexanitro-hexaazaisowurtzitane (HNIW).[8] A concerted unimolecular elimination of HONO seems to compete with the N−NO$_2$ homolysis in the gas-phase photolysis of RDX.[9]

The decomposition of RDX in the condensed phase involves several competing pathways. The slow thermal decomposition of RDX was studied by using the simultaneous thermogravimetric modulated beam mass spectrometry (STMBMS) technique, to measure the gas formation rates as a function of time.[10] These experiments revealed four different reaction channels. Two of the channels were first-order (i.e. unimolecular) pathways. A third channel involved bimolecular reaction between RDX and NO, as mentioned above. Finally, about 30% of the RDX was found to decompose through an autocatalytic mechanism, i.e., a free radical chain reaction.

The autocatalytic mechanism in the condensed phase is supported by observation of a kinetic isotope effect (KIE) for the global decomposition of liquid RDX-d_6.[11] The KIE measured for the global rate of energy release by using isothermal differential scanning calorimetry was found to be $k_H/k_{D_6} = 1.6$ at 232 °C. This primary deuterium KIE suggests that the rate is controlled by hydrogen (or deuterium) atom transfers that lead to formation of the RDX carbon radical. The combustion of RDX also shows a primary KIE = 1.4, as indicated from comparison of burn rates for RDX and RDX-d_6 at a pressure of 500 psig.[11] These observed KIEs support the

---

[⊗] Abstract published in *Advance ACS Abstracts,* June 1, 1997.

(1) Adams, G. F.; Shaw, R. W., Jr. *Annu. Rev. Phys. Chem.* **1992,** *43,* 311−340.

(2) (a) Zhao, X.; Hintsa, E. J.; Lee, Y. T. *J. Chem. Phys.* **1988,** *88,* 801−810. (b) Chambers, C. C.; Thompson, D. L. *J. Phys. Chem.* **1995,** *99,* 15881−15889.

(3) Botcher, T. R.; Wight, C. A. *J. Phys. Chem.* **1994,** *98,* 5441−44; **1993,** *97,* 9149−9153.

(4) Oxley, J. C.; Kooh, A. B.; Szekeres, R.; Zheng, W. *J. Phys. Chem.* **1994,** *98,* 7004−7008. Oxley, J. C.; Hiskey, M.; Naud, D.; Szekeres, R. *J. Phys. Chem.* **1992,** *96,* 2505−2509.

(5) Pace, M. D. *J. Phys. Chem.* **1991,** *95,* 5858−5864.

(6) Choi, M.; Kim, H.; Chung, C. *J. Phys. Chem.* **1995,** *99,* 15785−15789.

(7) Saxon, R. P.; Yoshimine, M. *J. Phys. Chem.* **1989,** *93,* 3130−3135. Lazarou, Y. G.; Papagiannakopoulos, P. *J. Phys. Chem.* **1990,** *94,* 7114−7119. Saxon, R. P.; Yoshimine, M. *Can. J. Chem.* **1992,** *70,* 572−579.

(8) Ryzhkov, L. R.; McBride, J. M. *J. Phys. Chem.* **1996,** *100,* 163−169. See also: Pace, M. D. *J. Energet. Mater.* **1985,** *3,* 279−291.

(9) Capellos, C.; Papagiannakopoulos, P.; Liang, Y. L. *Chem. Phys. Lett.* **1989,** *164,* 533−538. Zuckermann, H.; Greenblatt, G. D.; Haas, Y. *J. Phys. Chem.* **1987,** *91,* 5159−5161.

(10) Behrens, R., Jr.; Bulusu, S. *J. Phys. Chem.* **1992,** *96,* 8891−97, 8877−91. See also: Behrens, R., Jr.; Bulusu, S. *J. Phys. Chem.* **1991,** *95,* 5838−45. Behrens, R., Jr. *J. Phys. Chem.* **1990,** *94,* 6706−18. Behrens, R., Jr. in *Chemistry and Physics of Energetic Materials;* Bulusu, S. N., ed.; Kluwer: Dordrecht, 1990; pp 347−68.

notion that bimolecular hydrogen (or deuterium) atom transfers are rate-controlling processes in free radical chain reactions involved in RDX decomposition. The KIE experiments revealed that chemical reaction kinetics contribute to the global decomposition rate. Also, the experiments showed that hydrogen atom transfer is a rate determining step in both the slow decomposition and the combustion, so there is some mechanistic similarity in the two processes.
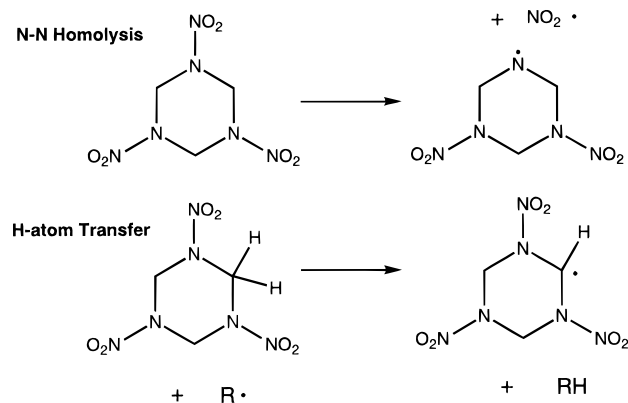
In a very recent study, a microprobe/mass spectrometer system was used to obtain species profiles in the gas phase during laser-induced combustion of RDX.[12] Concentrations of NO_2, N_2O, N_2, H_2, HCN, H_2O, CO, CO_2, and NO were measured as a function of height above the surface of burning RDX. These data are useful for developing a kinetic model for the combustion process.[13] Bimolecular reactions are effective during the acceleratory stage of the reaction, after the radical pool has been initiated. Some of the important secondary species in RDX decomposition are CH_2O, N_2O, NO, NO_2, and HCN. Reactions of these species are of general interest for understanding combustion of RDX and many other explosives.

The structure of RDX has been studied in the gas phase by electron diffraction,[14] in the α crystalline phase by neutron diffraction[15] and ^{14}N NQR spectroscopy,[16] and in solution by IR and NMR spectroscopy.[17] In the gas phase and the solid state RDX has a chair conformation. The gas-phase structure has C_{3v} symmetry, but has lower pseudo-C_s symmetry in the crystal. Rapid conformational interconversions take place in solution, so that only one signal is observed in the NMR spectrum even at −80 °C.[17] Classical molecular dynamics studies were made of RDX conformational interconversions,[18] and of the unimolecular decomposition of RDX.[2b] Ab initio studies were reported for the RDX chair conformers at the SCF level by using the minimal STO-3G and 4-21G basis sets.[19]

Clearly the N−NO_2 homolysis is a critical step for initiating RDX decomposition, and C−H homolysis (or H atom transfer)

is a critical step during radical chain reactions in the acceleratory stages of decomposition. In the present study, we use ab initio density functional theory to study the structures of the RDX nitrogen and carbon radicals. The use of gradient-corrected density functional theory is quite appropriate for computing accurate bond dissociation energies on large molecules.[20] Our results suggest the N−NO_2 and C−H bonds in RDX are unusually weak. The weak N−NO_2 bonds seem to be a consequence of destabilization of this bond by the nonreacting NO_2 substituents, and the weak C−H bonds result from stabilization of the carbon radical by the adjacent N−NO_2 functions. In addition, we report the optimized ab initio geometries for the RDX chair, boat and twist conformers. The computations suggest that several conformational energy minima exist within a small energy range of about 1 kcal/mol.

Methods

Computations were carried out with the GAUSSIAN 94 ab initio programs[21] on IBM RISC/6000 3BT workstations and on a Cray supercomputer. Optimized geometries and harmonic frequencies were computed at the RHF/6-31G* level of theory for closed shell molecules, and at the UHF/6-31G* level of theory for open shell radicals. The following abbreviations are used for brevity: dimethylnitramine (DMNA), 1-nitropiperidine (NPIP), hexahydro-1-nitro-1,3,5-triazine (NTA), hexahydro-1,3,5-trinitro-1,3,5-triazine (RDX), piperidine (PIP), hexahydro-*s*-triazine (TA), hexahydro-1,3-dinitro-1,3,5-triazine (DNTA), and cyclohexane (chex). The cyclic structures RDX, DNTA, NTA, TA, NPIP, PIP, and cyclohexane were computed in several different conformations. Each structure was reoptimized at the Becke3-Lee-Yang-Parr (B3LYP) hybrid density functional[20] level of theory, using the 6-31G* basis. Finally, single-point energies for the B3LYP/6-31G* geometries were computed at the B3LYP/6-311G** theoretical level. The standard 6-31G* and 6-311G** basis sets have been described elsewhere.[22] The absolute energies and RHF/6-31G* zero-point vibrational energies (ZPEs) for all structures are listed in Table 1. X−H bond dissociation energies (D_e) were computed by using the exact energy of 0.5 hartree for the hydrogen atom. Corrected bond energies (D_o) at 0 K were computed by adjusting D_e values for the zero-point vibrational energy (ZPE) difference with (U)HF/6-31G* frequencies scaled by 0.89. For comparison with experimental data, bond dissociation enthalpies at 298 K ($\Delta H°$) were computed by using thermal corrections[23] that are standard in the output from a GAUSSIAN frequency job. For computing X−H bond strengths, the exact energy of 0.5 hartree was used for the H atom, and the $\Delta H°$ value was corrected by adding $5/2 N_A k_B T$ (1.48 kcal/mol at 298 K) for the thermal contribution to the enthalpy of a monoatomic ideal gas.

Results

Ring Conformers. The various conformations for the cyclic structures, their symmetries, and their relative energies are shown in Figure 1. Chair conformers were optimized for chex, PIP, NPIP, TA, NTA, and DNTA (see Figure 1). Bond strengths for these six-membered cycles were computed to learn

(11) Trulove, P. C.; Chapman, R. D.; Shackelford, S. A. *Propellants Explos., Pyrotech.* **1994**, *19*, 42−58 and references therein. Shackelford, S. A. In *Chemistry and Physics of Energetic Materials* Bulusu, S. N., Ed.; Kluwer: Dordrecht, 1990; pp 413−432.

(12) Litzinger, T. A.; Fetherolf, B. L.; Lee, Y. J.; Tang, C. J. *J. Propul. Power* **1995**, *11*, 698−703.

(13) Yetter, R. A.; Dryer, F. L.; Allen, M. T.; Gatto, J. L. *J. Propul. Power* **1995**, 11, 683−697. Melius, C. F. In *Chemistry and Physics of Energetic Materials* Bulusu, S. N., Ed.; Kluwer: Dordrecht, 1990, pp 21−78.

(14) Choi, C. S.; Prince, E. *Acta Crystallogr.* **1972**, *B28*, 2857.

(15) Shishkov, I. F.; Vilkov, L. V.; Kolonits, M.; Rozsondai, B. *Struct. Chem.* **1991**, *2*, 57−64.

(16) Karpowicz, R. J.; Brill, T. B. *J. Phys. Chem.* **1984**, *88*, 348−352.

(17) Karpowicz, R. J.; Brill, T. B. *J. Phys. Chem.* **1983**, *87*, 2109−2112.

(18) Wallis, E. P.; Thompson, D. L. *J. Chem. Phys.* **1993**,*99*, 2661−2673.

(19) (a) Habibollahzadeh, D.; Grodzicki, M.; Seminario, J. M.; Politzer, P. *J. Phys. Chem.* **1991**, *95*, 7699. (b) Coffin, J. M.; Newton, S. Q.; Ewbank, J. D.; Schafer, L.; Alsenoy, C. V.; Siam, K. *J. Mol. Struct.* **1991**, *251*, 219.

(20) (a) Stephens, P. J.; Devlin, F. J.; Chabalowski, C. F.; Frisch, M. J. *J. Phys. Chem.* **1994**, *98*, 11623. (b) Becke, A. D. *J. Chem. Phys.* **1993**, *98*, 5648−5652. 1372; **1992**, *96*, 2155; **1992**, *97*, 9173.

(21) Gaussian 94, Revision B.1, Frisch, M. J.; Trucks, G. W.; Schlegel, H. B.; Gill, P. M. W.; Johnson, B. G.; Robb, M. A.; Cheeseman, J. R.; Keith, T.; Petersson, G. A.; Montgomery, J. A.; Raghavachari, K.; Al-Laham, M. A.; Zakrzewski, V. G.; Ortiz, J.V.; Foresman, J. B.; Cioslowski, J.; Stefanov, B. B.; Nanayakkara, A.; Challacombe, M.; Peng, C. Y.; Ayala, P. Y.; Chen, W.; Wong, M. W.; Andres, J. L.; Replogle, E. S.; Gomperts, R.; Martin, R. L.; Fox, D. J.; Binkley, J. S.; Defrees, D. J.; Baker, J.; Stewart, J. P.; Head-Gordon, M.; Gonzalez, C.; Pople, J. A. Gaussian, Inc.: Pittsburgh, PA, 1995.

(22) (a) Frisch, M. J.; Frisch, A.; Foresman, J. B. *Gaussian 94 User's Reference*; Gaussian, Inc.: Pittsburgh, 1994. (b) Hehre, W. J.; Radom, L.; Schleyer, P. v. R. *Ab Initio Molecular Orbital Theory*; Wiley-Interscience: New York, 1986.

(23) McQuarrie, D. A. *Statistical Thermodynamics*; Harper and Row: New York, 1973.

D_o for Hexahydro-1,3,5-trinitro-1,3,5-triazine

J. Am. Chem. Soc., Vol. 119, No. 28, 1997 6585
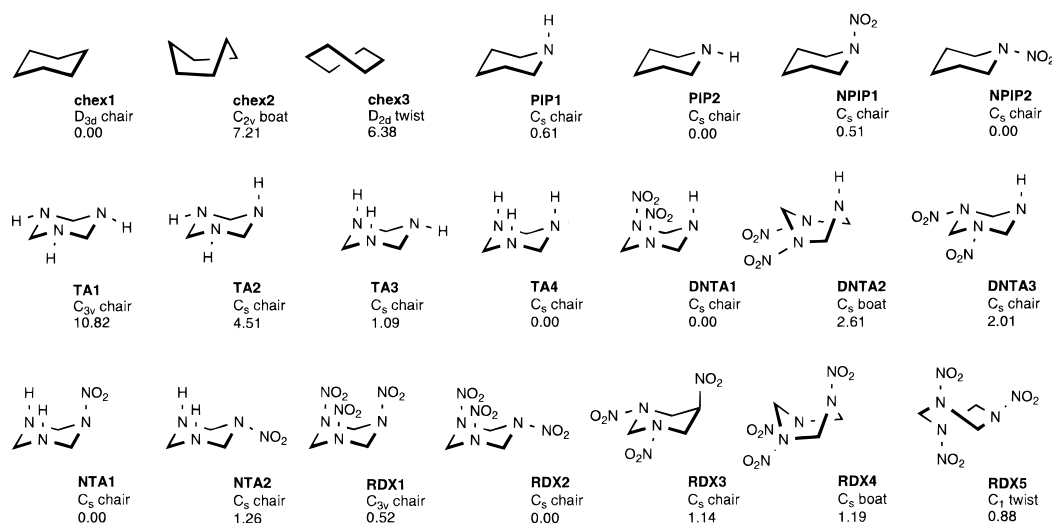
Figure 1. Conformations of cyclic structures, their symmetry point groups and relative energies (B3LYP/6-311G**) in kcal/mol.

Table 1. Energies in Atomic Units (1 hartree = 627.51 kcal/mol)[a]

	RHF/A	B3LYP/A	B3LYP/B	ZPE
chex1 (chair)	−234.20801	−235.88043	−235.94422	0.182433
chex2 (boat)	−234.19554	−235.86876	−235.93273	0.182254
chex3 (twist)	−234.19723	−235.87005	−235.93405	0.182386
chex-rad (0.76)	−233.57994	−235.21387	−235.27716	0.166940
PIP1	−250.18741	−251.90382	−251.97389	0.170943
PIP2	−250.18871	−251.90437	−251.97489	0.171098
NPIP1	−453.64969	−456.39810	−456.52201	0.175163
NPIP2	−453.65076	−456.39861	−456.52282	0.174915
PIP-Nrad (0.76)	−249.57591	−251.25030	−251.31557	0.156022
TA1 (EEE)	−282.14329	−283.94510	−284.02995	0.147738
TA2 (AEE)	−282.15406	−283.95594	−284.04001	0.148394
TA3 (AAE)	−282.15946	−283.96172	−284.04546	0.148755
TA4 (AAA)	−282.16023	−283.96316	−284.04720	0.148721
TA-Nrad1 (0.76)	−281.54461	−283.30487	−283.38361	0.133339
TA-Nrad2 (0.76)	−281.53363	−283.29291	−283.37250	0.132568
TA-Crad1 (0.76)	−281.53203	−283.30139	−283.38604	0.132775
TA-Crad2 (0.76)	−281.53077	−283.30198	−283.38686	0.133220
TA-Crad3 (0.76)	−281.53683	−283.30756	−283.39232	0.134134
NTA1	−485.62138	−488.45617	−488.59371	0.152658
NTA2	−485.61995	−488.45369	−488.59170	0.152205
DNTA1	−689.06820	−692.93671	−693.12803	0.155760
DNTA2	−689.06524	−692.93193	−693.12387	0.155092
DNTA3	−689.06657	−692.93266	−693.12483	0.155247
RDX1	−892.50534	−897.40894	−897.65465	0.158421
RDX2	−892.50707	−897.40939	−897.65548	0.158653
RDX3	−892.50690	−897.40723	−897.65367	0.158570
RDX4	−892.50652	−897.40766	−897.65359	0.158557
RDX5	−892.50664	−897.40833	−897.65408	0.158700
RDX-Crad (0.84)	−891.88366	−896.76029	−897.00600	0.143388
RDX-Nrad1 (0.76)	−688.44229	−692.27024	−692.45721	0.139951
RDX-Nrad2 (0.76)	−688.44201	−692.26868	−692.45554	0.139247
DMNA	−337.70106	−339.65655	−339.75319	0.103639
Me$_2$N (0.76)	−133.62760	−134.50949	−134.54759	0.083594
Me$_2$NH	−134.23885	−135.16285	−135.20540	0.099455
NH$_2$NO$_2$	−259.63941	−261.03150	−261.11362	0.043663
NO$_2$ (0.77)	−204.03149	−205.07221	−205.13247	0.009853
NH$_2$ (0.76)	−55.55770	−55.87262	−55.89507	0.020565

[a] Basis sets: A = 6-31G*; B = 6-311G**. ZPE is unscaled RHF/6-31G* zero-point vibrational energy. UHF/6-31G* values for $\langle S^2 \rangle$ in parentheses.

the structural factors that influence the C−H and N−NO$_2$ bond strengths in RDX (see discussion below and Chart 1).

Cyclohexane (chex) was computed in the chair, boat, and twist conformations. The C_{2v} boat is a transition structure for interconversion of twist conformers. This differs from the RDX boat conformer, which is a local energy minimum. The 6.4 kcal/mol twist−chair energy difference in cyclohexane is considerably larger than the 1.2 kcal/mol difference in RDX.

Hexahydro-s-triazine (TA) was computed in four conformations differing in the number of axial N−H bonds. Anomeric stabilization leads to a large energy preference (11 kcal/mol−see Figure 1) for the triaxial conformer **TA4** compared to the triequatorial conformer **TA1**. The energies change in the order AAA < AAE < AEE < EEE (A = axial, E = equatorial). The preference for axial N−H orientation was noted in a previous ab initio study,[24] and is attributed to anomeric type stabilization.[24] That is, the equatorial N lone pairs are aligned favorably for interaction with the adjacent C−N antibonding orbitals. A similar preference for the axial orientation of amine substituents is found in other hexahydro-s-triazines.[25] For example, hexahydro-1,3,5-trimethyl-1,3,5-triazine exists as a 1/1 mixture of the diaxial and monoaxial conformers, with no molecules having the triequatorial conformation.[25b]

Piperidine (PIP) was computed in the axial and equatorial N−H conformations, and 1-nitropiperidine (NPIP) was similarly computed in the axial and equatorial N−NO$_2$ conformations. These molecules have only one heteroatom in the ring, and in the absence of the anomeric effect the equatorial conformers **PIP2** and **NPIP2** are favored slightly (Figure 1).

NTA was computed in two chair conformations, differing in the axial/equatorial orientation of the nitro group. In both **NTA1** and **NTA2** the two equivalent N−H bonds are axial. Other NTA conformers having one or both N−H bonds equatorial were not computed, but these would presumably be higher in energy than the diaxial conformers.

DNTA was computed in two chair conformations. Both conformers have the N−H bond axial. In **DNTA1** the two equivalent NO$_2$ groups are axial and in **DNTA2** they are equatorial. In addition a C_s boat conformer **DNTA2** was computed. As with NTA, chair structures having the N−H bond equatorial were not computed, but these are presumably less stable than the N−H axial structures.

RDX Conformers. The five RDX conformers are the triaxial chair (C_{3v}), diaxial chair (C_s), monoaxial chair (C_s), boat (C_s), and twist (C_1) (see Figure 2). Each is a local minimum. It was attempted to locate a fourth chairlike conformation having all three NO$_2$ groups equatorial, but this structure converted to

(24) (a) Carballeira, L.; Fernandez, B.; Mosquera, R. A.; Rios, M. A.; Otero, J. R.; Vazquez, S. *J. Mol. Struct. (Theochem)* **1990**, *205*, 223−234. (b) Carballeira, L.; Mosquera, R. A.; Rios, M. A. *J. Mol. Struct.* **1989**, *195*, 89−101.

(25) (a) Jones, R. A. Y.; Katritzky, A. R.; Snarey, M. *J. Chem. Soc. (B)* **1970**, 135−138. (b) Bushweller, C. H.; Lourandos, M. Z.; Brunelle, J. A. *J. Am. Chem. Soc.* **1974**, *96*, 1591−1593. (c) Hutchins, R. O.; Kopp, L. D.; Eliel, E. L. *J. Am. Chem. Soc.* **1968**, *90*, 7174−7175.

Table 2. Theoretical (RHF/6-31G* and B3LYP/6-31G*) and Experimental Geometries for C_{3v} Conformer **RDX1** and C_s Conformer **RDX2** (bond lengths in Å, bond angles in deg)

	RHF	B3LYP	expt		RHF	B3LYP	expt
			(a) C_{3v} Conformer **RDX1**[a]				
CN	1.452	1.460	1.464(6)	NCN	111.6	112.7	109.4(6)
NN	1.370	1.422	1.413(5)	CNC	115.3	115.5	123.7(6)
NO	1.189	1.222	1.213(2)	NNO	116.9	116.4	117.2
CNN	118.6	117.5	116.3(5)	α[b]	26.3	30.2	19(2)

Numbering Scheme

	RHF	B3LYP	expt		RHF	B3LYP	expt
			(b) C_s Conformer **RDX2**[c]				
N1C2	1.464	1.473	1.457(3)	C2N3C4	115.2	115.5	114.7(2)
C2N3	1.442	1.449	1.441(3)	N3C4N5	111.5	112.7	111.7(2)
N3C4	1.453	1.462	1.463(3)	C2N1N7	115.5	115.2	120.3(2)
N1N7	1.362	1.402	1.351(3)	C2N3N10	117.1	116.0	116.3(2)
N3N10	1.377	1.432	1.395(2)	C4N3N10	117.6	116.5	117.0(2)
N7O8	1.191	1.226	1.221(4)	N1N7O8	117.0	116.6	117.6(2)
N10O11	1.189	1.221	1.206(4)	N3N10O11	117.1	116.6	116.9(2)
N10O12	1.187	1.220	1.202(4)	N3N10O12	116.5	116.2	117.2(2)
C6N1C2	115.1	115.0	115.1(2)	α_1[d]	36.7	37.7	19.8
N1C2N3	108.6	109.2	108.1(2)	α_3[d]	30.8	33.9	33.6

[a] Experimental Gas Phase Geometry from: Shishkov, I. F.; Vilkov, L. V.; Kolonits, M.; Rozsondai, B. *Struct. Chem.* **1991**, *2*, 57−64. [b] Amine pyramidalization angle. [c] Average experimental geometric parameters for α-crystalline RDX from: Choi, C. S.; Prince, E. *Acta Crystallogr.* **1972**, *B28*, 2857. [d] Amine pyramidalization angles at N1 and N3.
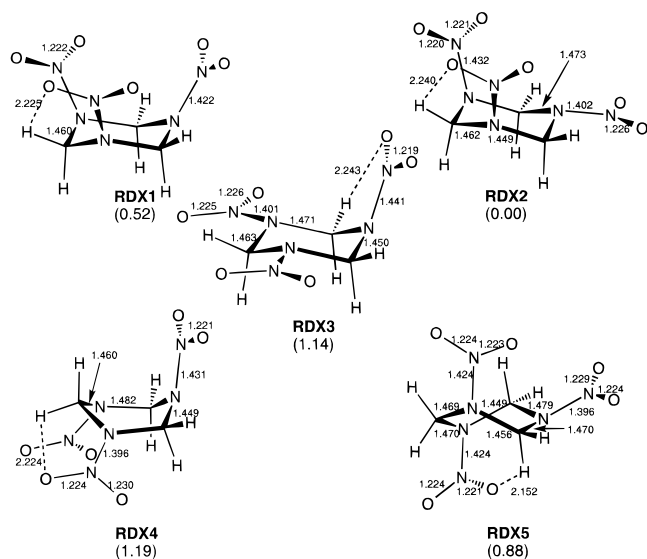
Figure 2. Conformations of RDX. Selected B3LYP/6-31G* bond lengths (Å) and B3LYP/6-311G** relative energies (kcal/mol) are given.

the triaxial conformer **RDX1** when the geometry was optimized. Previous calculations at the RHF/4-21G level indicated that the C_{3v} structure **RDX1** was the only stable chair conformer.[24b] The global minimum is diaxial chair **RDX2**, but the computed range in energy for the five conformers is only about 1 kcal/mol (Figure 1).[18] This is smaller than a previously predicted energy difference of 4.5 kcal/mol between the chair and boat RDX conformers, based on a classical force field.[18]

The energy range in the RDX conformers is much smaller than that for the hexahydro-*s*-triazine (TA) conformers (Figure 1). The anomeric effect is attenuated in RDX conformers by donation from the N lone pairs into the NO_2 groups, which

makes the lone pairs less available for anomeric type interaction. Still, the effect does contribute to stabilizing the axial NO_2 orientation, and also leads to lengthening of the axial NN bonds in **RDX2** and **RDX3** (see Figure 2).[24]

The amine inversion barrier in RDX and other nitramines is quite small.[26] For example, the computed barrier in the parent nitramine, NH_2NO_2, is 0.81 kcal/mol (B3LYP/6-311G** + ZPE). The inversion period in solution or the gas phase should be on the same time scale as for internal rotations with similar barriers, of the order 10^{-10} s. Clearly the chair conformers differing in axial/equatorial NO_2 orientation will be averaged during an infrared or nuclear magnetic resonance experiment.[16] Then the effective structure for the RDX chair in the gas phase or solution is the more symmetrical C_{3v} geometry with three equivalent nitro groups. Besides the rapid amine inversion, proton NMR experiments reveal that ring conformational inversion is fast even at −80 °C.[16]

The situation is changed in the solid state, where the molecular conformation is fixed. The observed conformation for RDX in the α phase crystal is similar to that for **RDX2**.[14] The experimental structure has C_s pseudosymmetry, with two nearly equivalent axial nitro groups. The low symmetry in the observed structure is no doubt due to crystal packing effects. The observed geometry of gas-phase RDX[15] has a (time averaged) C_{3v} chair conformation as in **RDX1**. The experimental and theoretical RDX structures are compared in Table 2. In the observed gas-phase structure the C−N−C angles are 8° larger and the N−C−N angles are 3° smaller than in the B3LYP/6-31G* structure, and the amine pyramidalization (α) is 11° smaller in the experimental structure (Table 2, part A). The observed crystal structure has shorter N−N bonds by 0.03− 0.05 Å than in the B3LYP/6-31G* structure (Table 2, part B),

(26) Ritchie, J. P. *J. Am. Chem. Soc.* **1989**, *111*, 2517−2520.
(27) Scott, A. P.; Radom, L. *J. Phys. Chem.* **1996**, *100*, 16502−16513.

but the long axial N−N bonds are evident in both the experimental and theoretical geometries. Once again the N1 pyramidalization angle α_1 is smaller in the observed structure than the B3LYP structure by 18°.

Intermolecular electrostatic interactions[17] contribute to the short N−N bonds in the crystal, as was mentioned in a previous comparison of theoretical and experimental geometries for dimethylnitramine.[28] Donation from the amine lone pairs into the nitro groups leads to increased polarity in the solid state. This enhances electrostatic N−O attractions between the NO_2 groups of adjacent molecules. Short intermolecular N−O distances of ca. 3.1 Å found in crystalline RDX give evidence for such interactions.[17]
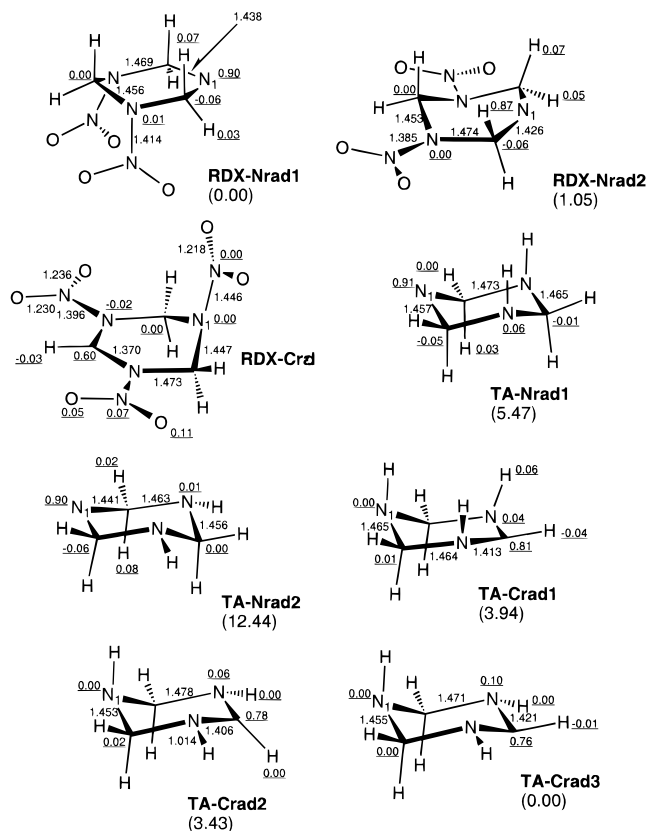
Besides the *intermolecular* N−O nonbonded contacts, the theoretical geometries have *intramolecular* O−H nonbonded contacts (i.e. hydrogen bonds) between the NO_2 oxygens and the CH_2 hydrogens. The nonbonded O−H distances are ca. 2.2 Å (Figure 2). The interactions are significant in view of suggestions that intramolecular hydrogen transfer is a minor pathway for decomposition of RDX and other nitramines.[4,9]

The B3LYP/6-31G* harmonic vibrational frequencies and their assignments for C_{3v} conformer **RDX1** and the experimental frequencies[12] for vapor phase RDX are given in the Supporting Information. The strongest bands are the NO_2 stretching vibrations which appear at 1704 and 1370 cm^{-1} in the theoretical spectrum. These are in reasonable agreement with the observed bands at 1584 and 1268 cm^{-1}, after allowance is made for anharmonic effects that make the observed fundamentals smaller than the harmonic frequencies by ca. 5%.[27] The B3LYP/6-31G* zero-point vibrational energy for **RDX1** is 89.9 kcal/mol, which after scaling[27] by 0.96 reduces to 86 kcal/mol. This agrees reasonably with a recent estimate of 80 kcal/mol.[2b]

Carbon and Nitrogen Radicals. The conformations for the N- and C-radicals from RDX and TA are shown in Figure 3. The RDX nitrogen radical **RDX-Nrad1** has a conformation intermediate between the chair and half-chair. This is more stable by 1.04 kcal/mol than the half-chair/boat conformer **RDX-Nrad2**. The B3LYP/6-311G** atomic spin densities (Figure 3) show that the N radicals hyperconjugate with the adjacent C−H bonds.[28] Similar hyperconjugation is evident in **TA-Nrad2**, particularly for the axial C−H bond (Figure 3).

RDX-Crad has the half-chair conformation, with all ring atoms coplanar except N1. The (NO2)NCN(NO2) moiety forms an extended π-framework, over which the radical at C4 is delocalized into the two adjacent NO_2 groups (Figure 3). The delocalized π system leads to the short C−N bonds (1.37 Å), short N−N bonds (1.40 Å), and wide (118°) N−C−N angle at the radical center. Delocalization of the radical also contributes to the small C−H bond dissociation energy in RDX.

In contrast to the planar radical in **RDX-Crad**, the TA carbon radicals are slightly pyramidal (Figure 3). In **TA-Crad1** the N−H bonds adjacent to the radical are axial, while in **TA-Crad2** and **TA-Crad3** they are equatorial. The global minimum is **TA-Crad3**, which is more stable than **TA-Crad1** and **TA-Crad2** by 3.9 and 3.4 kcal/mol, respectively. The energetic preference for the equatorial N−H orientation in **TA-Crad3** is in contrast with the 11 kcal/mol preference for axial N−H bonds in the TA conformers (Figure 1). The favorable orbital interaction of the C-radical with the adjacent axial N lone pairs[29] opposes the anomeric stabilization[24a] of the axial N−H conformer.

(28) Harris, N. J.; Lammertsma, K. *J. Phys. Chem. A* **1997**, *101*, 1370−1373.

(29) Steigerwald, M. L.; Goddard, W. A., III; Evans, D. A. *J. Am. Chem. Soc.* **1979**, *101*, 1994-1997.

Figure 3. Carbon and nitrogen radicals from RDX and hexahydro-*s*-triazine (TA). Selected B3LYP/6-31G* bond lengths (Å), B3LYP/6-311G** atomic spin densities (underlined), and B3LYP/6-311G** relative energies for isomeric structures (kcal/mol) are given.

Table 3. Comparison of Theoretical and Experimental Dissociation Energies for N−N, N−H, and C−H bonds[a]

| | G2 | | B3LYP/6-311G** | | |
	D_o	$\Delta H°$	D_o	$\Delta H°$	expt $\Delta H°$ (ref)
NH₂−NO₂	51.1	53.0	46.6	48.5	
MeNH−NO₂	51.7	53.1	44.5	45.9	
NH₂−H	106.5	107.9	104.4	105.8	104 ± 2 (32)
Me₂N−H	93.7	95.3	90.2	91.8	94.9 ± 2 (32)
Me₂CH−H	98.5	100.3	95.5	97.3	96.1 ± 1 (33, 34)
C₆H₁₁−H			96.2	97.8	95.9 ± 1 (33, 34)

[a] D_o is the bond energy at 0 K, corrected for ZPVE; $\Delta H°$ is the bond enthalpy at 298 K.

Bond Strengths. The accuracy of bond dissociation energies computed with B3LYP/6-311G** was checked by computing D_o for several small test molecules using accurate Gaussian-2 (G2) theory.[30] The G2 theory is an approximation to the QCISD(T)/6-311+G(3df,2p)//MP2/6-31G* level of theory, and is intended to calculate atomization energies accurate to within 1−2 kcal/mol.[30] The G2, B3LYP, and experimental strengths for N−N, N−H, and C−H bonds of the test molecules are presented in Table 3. For purposes of comparison with experiment, the B3LYP and G2 bond energies (D_o) at 0 K were corrected to bond enthalpies ($\Delta H°$) at 298 K.

The B3LYP N−N bond energies in Table 3 appear underestimated by ca. 6 kcal/mol compared with G2 bond energies. The tendency for B3LYP to underestimate N−N bond energies in nitramines is not surprising, considering our earlier finding that B3LYP underestimates the C−N bond energy in CH_3NO_2

(30) Gaussian-2 theory: Curtiss, L. A.; Carpenter, J. E.; Raghavachari, K.; Pople, J. A. *J. Chem. Phys.* **1992**, 96, 9030. Curtis, L. A.; Jones, C.; Trucks, G. W.; Raghavachari, K.; Pople, J. A. *J. Chem. Phys.* **1990**, *93*, 2537.

Table 4. Bond Dissociation Energies (kcal/mol) at 0 K[a]

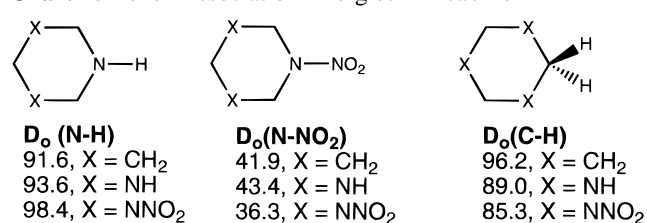|	D_e			
	RHF/A	B3LYP/A	B3LYP/B	D_o
A. N−NO₂ Bond Strengths in Nitramines				
DMNA	26.33	46.97	45.89	40.20
NPIP	27.20	47.76	46.92	41.87
NTA	28.41	49.63	48.71	43.42
RDX	20.88	42.01	41.29	36.35
B. N−H Bond Strengths in Amines				
PIP	70.78	96.68	99.98	91.56
TA	72.55	99.33	102.65	93.61
DNTA	79.01	104.46	107.19	98.38
C. Secondary C−H Bond Strengths				
chex	80.36	104.51	104.83	96.18
TA	77.44	97.64	97.19	89.04
RDX	77.44	93.56	93.81	85.28

[a] Basis sets: A = 6-31G*; B = 6-311G** D_o is corrected for ZPVE using 0.89 scaled UHF/6-31G* frequencies, D_e is uncorrected.

by 9 kcal/mol.[31] The B3LYP N−H bond strengths (Table 4) are also too small by ca. 3 kcal/mol compared with the G2 bond strengths. Compared with the experimental[32] N−H bond enthalpies the B3LYP values for $\Delta H°$ are 1.8 kcal/mol too large (NH₃) and 3.1 kcal/mol too small (Me₂NH). The B3LYP C−H bond energy in propane (carbon-2) is underestimated by 3.0 kcal/mol compared with the G2 bond strength. The experimental C−H bond dissociation enthalpies for propane and cyclohexane (Table 3) were calculated by using heats of formation for cyclohexane (−29.5 kcal/mol),[33] propane (−24.9 kcal/mol),[33] 2-propyl (19.1 ± 0.6 kcal/mol),[34] and cyclohexyl (14.3 ± 1.0 kcal/mol),[34] and the bond dissociation enthalpy for H₂ (104.21 kcal/mol).[32] The B3LYP C−H bond enthalpies appear overestimated by ca. 1.5 kcal/mol compared with the experimental bond enthalpies in Table 3.

In summary, the computed B3LYP/6-311G** strengths for N−H and C−H bonds agree reasonably with experimental bond enthalpies and with accurate bond energies computed with G2 theory. However, the N−N bond strengths in nitramines are underestimated by about 6 kcal/mol by B3LYP/6-311G**.

Presented in Table 4 are dissociation energies for N−NO₂ bonds (part A), N−H bonds (part B), and C−H bonds (part C). The bond strengths are based on the lowest energy conformers for the closed shell molecules and the product radicals. After correcting for the B3LYP/6-311G** underestimation of N−NO₂ bond strengths, our best estimate for D_o(N−NO₂) in RDX is 42 kcal/mol.

Some insights are gained from comparing the N−NO₂ and N−H bond strengths in Tables 3 and 4. The weaker bonds in DMNA and Me₂NH compared with NH₂NO₂ and NH₃ are a consequence of the greater stability of the Me₂N radical than the NH₂ radical. When the secondary N-radical is incorporated into a six-membered ring, as in the PIP N-radical, the D_o(N−H) and D_o(N−NO₂) values are both increased by ca. 1.5 kcal/mol. Substitution of two CH₂ groups in PIP by two N−H groups in TA causes a further increase in D_o(N−H) by 2.0 kcal/mol. Similarly, substitution of CH₂ in NPIP for N−H in NTA causes an increase in D_o(N−NO₂) by 1.5 kcal/mol. These relationships are depicted in Chart 1. The most interesting comparison is in D_o(N−H) for DNTA and TA, and D_o(N−NO₂) in NTA and RDX. In the former case, substitution of N−NO₂ in DNTA for N−H in TA causes a 4.8 kcal/mol increase in

(31) Harris, N. J.; Lammertsma, K. *J. Am. Chem. Soc.* **1996**, *118*, 8048−8055.
(32) Dean, J. A. *Lange's Handbook of Chemistry*, 14th ed; McGraw-Hill: New York, 1992.
(33) DeTar, D. F. *J. Org. Chem.* **1995**, *60*, 7125−7133.
(34) Liu, R.; Allinger, N. L. *J. Comput. Chem.* **1994**, *15*, 283−299.

Chart 1. Bond Dissociation Energies in kcal/mol

D_o (N-H)
91.6, X = CH₂
93.6, X = NH
98.4, X = NNO₂

D_o(N-NO₂)
41.9, X = CH₂
43.4, X = NH
36.3, X = NNO₂

D_o(C-H)
96.2, X = CH₂
89.0, X = NH
85.3, X = NNO₂

D_o(N−H). In the latter case, substitution of N−NO₂ in RDX for N−H in NTA causes a 7.1-kcal/mol decrease in D_o(N−NO₂). Thus, the replacement of N−H by the electron withdrawing N−NO₂ functional group has opposite effects on the strengths of the N−H and N−NO₂ bonds (Chart 1).

The C−H bond strengths in Table 4, part C, illustrate the stabilization of carbon radicals by α-amine and α-nitramine substituents. The C−H bond strengths in propane and cyclohexane are nearly the same, showing that incorporating the secondary C-radical into a six-membered ring has little effect on the radical stability. The C−H bond strength is 7.2 kcal/mol lower in TA than in cyclohexane, and the C−H bond strength in RDX is 10.9 kcal/mol lower than in cyclohexane. Thus the replacement of CH₂ by α-N−H leads to a decrease in C−H bond strength, and replacement of α-N−H by α-N−NO₂ leads to a further decrease (Chart 1). These results are explained by a bonding interaction between the C-radical and the adjacent amine lone pairs (in the case of TA). Further stabilization of the RDX C-radical is expected because of delocalization of the radical into the two NO₂ groups. Evidence for such delocalization is seen from the analysis of the geometry and spin densities in the RDX carbon radical, discussed above.

Conclusions

Our best calculations using the B3LYP/6-311G**//B3LYP/6-31G* theoretical level suggest that the gas-phase RDX molecule exists as a mixture of chair, boat, and twist conformers. The range in energy for these conformers is only about 1 kcal/mol. Three energy minimum chair conformations were found, differing in the axial/equatorial orientations of the nitro groups. Because of the low barrier for nitramine inversions, these three conformers should interconvert quite rapidly, giving an average chair structure with three equivalent nitro groups and C_{3v} symmetry. This is in agreement with the experimentally observed gas-phase structure for RDX. The observed conformation for crystalline RDX is similar to the conformation for the theoretical global energy minimum structure. Differences between observed and theoretical N−N bond lengths in RDX can be explained by crystal packing effects. Intermolecular electrostatic interactions in the solid state favor resonance donation of the amine lone pair into the NO₂ group, leading to shorter N−N bonds than in the gas phase. The RDX molecule has short intramolecular O−H contacts, which suggests that RDX can react by elimination of HONO.

Our estimated C−H and N−NO₂ bond dissociation energies (D_o) for RDX are respectively 85 and 42 kcal/mol. The latter value includes a correction for the tendency for B3LYP/6-311G** theory to underestimate N−NO₂ bond strengths by 6 kcal/mol compared with high level G2 theory. These are smaller than typical secondary C−H and N−NO₂ bond strengths in cyclohexane (96 kcal/mol) and DMNA (46 kcal/mol, our best estimate). Thus, the initiation of RDX decomposition by N−NO₂ homolysis and propagation of the decomposition by hydrogen atom abstractions should be facile processes. The low N−NO₂ bond strength is a consequence of the σ electron

withdrawing NO_2 substituents in RDX. The weak C−H bond in RDX is similar in strength to an allylic or benzylic C−H bond, rather than a typical aliphatic C−H bond. The geometric features and atomic spin densities in the RDX carbon radical show it is partly delocalized into the adjacent NO_2 groups.

Supporting Information Available: B3LYP/6-31G* internal coordinate geometries for RDX conformers, and for RDX carbon and nitrogen radicals; B3LYP/6-31G* harmonic frequencies together with experimental frequencies for gas-phase RDX; summary of G2 energies used in computing bond dissociation energies for propane, dimethylamine, methylnitramine, and nitramine (6 pages). See any current masthead page for ordering and Internet access instructions.

JA970392I